

A 2-D imaging dosimeter for photodynamic therapy

Y. Zhao^a, M. Hinds^a, T. Moritz^a, J. Gunn^b, B. W. Pogue^b, and S. J. Davis^a

a) Physical Sciences Inc., 20 New England Business Center, Andover, MA USA 01810-1077

b) Dartmouth College, Thayer School of Engineering, 8000 Cummings Hall, Hanover, NH USA
03755-8001

ABSTRACT

Photodynamic Therapy (PDT) is a promising modality for cancer treatment. Typically, a laser is used to photo-excite a photosensitizer (PS) that subsequently collides with oxygen molecules promoting them to the metastable singlet delta state $O_2(^1\Delta)$. Singlet oxygen molecules are believed to be the species that destroys cancerous cells during PDT. In this paper we describe a novel 2D imaging sensor for photosensitizer fluorescence and singlet oxygen luminescence. We describe our instrument and initial results from both *in-vitro* and *in-vivo* studies that indicate that this system may be a valuable dosimeter for both PDT researchers and eventually for clinical application.

Keywords: photodynamic therapy, photosensitizer, singlet oxygen, optical detection, imaging

1. INTRODUCTION

Photodynamic Therapy, PDT, uses light and selective photosensitizers to visualize and treat tumors.¹⁻⁷ The treatment administers a PS drug either systemically or topically. The PS is selectively retained in tumors. Upon irradiation with light of an appropriate wavelength that matches the strong singlet-singlet absorption band of the PS, a metastable triplet state of the PS is populated by an intra-system energy transfer. This metastable triplet state collisionally transfers its energy to O_2 molecules within the tumor promoting the ground state O_2 to the $O_2(^1\Delta)$ state that is responsible for the cell destruction by: a) direct damage to cell walls and mitochondria,⁶ and b) vascular constriction that starves the tumor of nutrients.⁷ Singlet oxygen is implicated in both mechanisms. The Type II singlet oxygen production mechanism is shown in Figure 1.

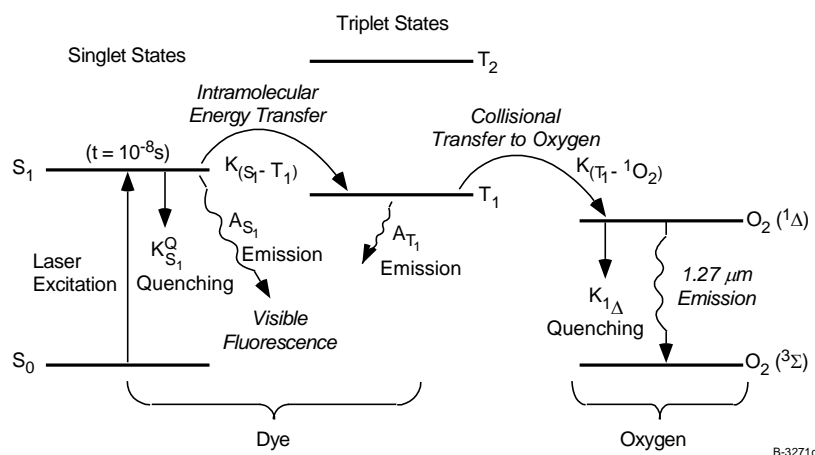


Figure 1. The Type II production mechanism for singlet oxygen.

FDA approval has been granted for treatment of esophageal adenocarcinoma and high-grade dysplasia and certain lung cancers. PDT is being used in clinical trials for bladder, brain, skin and other cancers. PDT is also being applied to important areas outside of cancer treatment including age related macular degeneration and actinic keratosis, a pre-cancerous skin condition. The tumor responses of PDT have been highly variable patient to patient. PDT treatment

depends upon several parameters: the PS concentration in the tumor, treatment light intensity, total light dose (fluence), and tumor oxygenation; and key ones are not measured. The singlet O_2 monitoring is a direct measure of the PDT dose defined as the available molecular O_2 multiplied by the PS concentration and the light fluence: $PDT\ dose = \int [PS(t)] * [O_2] \Phi(t) dt$. Currently, there are no *in vivo* capable singlet dosimeters during PDT treatment, so these key parameters of PDT treatment are unknown to physicians in the clinic, and this likely contributes to variability in treatment outcomes. Indeed, dosimetry is arguably the most important unresolved active area in PDT,⁸⁻³⁶ and an accurate dosimeter to characterize and optimize the individual treatment response of PDT in a clinical environment would be an important tool to improve PDT efficacy.

A number of groups have attempted to develop dosimeters based only on the fluorescence intensity of the PS in the tumor,^{14-16,19,20} but the complex dynamics of oxygen-independent photo-bleaching of the PS as well as photoproduct formation may preclude this as an accurate method without careful calibration for each indication. Accurate dosimetry for PDT continues to be both a challenge and an obstacle for further development.⁸⁻³⁶ Optical measurement of the singlet O_2 emission produced in tissue is a more direct and complementary way to assess PDT dose to the tissue. It is well established that the PDT process consumes oxygen in a manner which can substantially deplete the available oxygen supply within tumor tissues.^{8,21} This effect is unfavorable for maximal treatment response, as it results in decreased singlet O_2 production. It has been suggested that maximizing the oxygenation of tissue can enhance PDT efficiency.²² Previously, we⁸⁻¹³ and others^{15,23-25,29} have used pulsed lasers and temporal discrimination to detect singlet oxygen.

In the past we have used a set of three, 15 nm bandwidth optical filters (1.22, 1.27, and 1.32 μm) to spectrally discriminate the singlet O_2 emission signal and PS fluorescence and other background signals. The emissions at 1.22 and 1.32 μm contain only PS fluorescence and the emission at 1.27 μm contains contributions from both the singlet O_2 and PS. We used the average of the signals at 1.22 and 1.32 μm and subtracted it from the signal at 1.27 μm to recover the singlet oxygen component. To better discriminate against the PS fluorescence we developed a pulsed approach described in several papers.⁸⁻¹³ In brief, we modulate the diode laser with a square wave, typically with a 5 μs width and at repetition rates from 10 to 40 kHz. Even during the diode laser pulse the peak power is only 3-20 mW depending on the pulsewidth. The PS fluorescence has a lifetime of less than 10 ns and promptly follows the diode laser pulse. In contrast, the singlet oxygen luminescence is a strictly forbidden transition and in water has a lifetime of approximately 4 μs .⁸ In tissue this is reduced to 0.3 to 0.5 μs due to severe quenching by tissue²³⁻²⁵. While this rapid quenching in tissue creates a challenge for measuring the singlet oxygen, it is this rapid quenching that causes the PDT effects of cell death and reduction of blood flow to the tumor.

Figure 2 shows *in-vitro* data obtained with a non-imaging near-IR photomultiplier tube (PMT)-based system.⁸ We set the photon counter to gate after the termination of the diode laser pulse. The emission at 1.22 and 1.32 μm follows the diode laser pulse shape due to the < 10 ns PS fluorescence lifetime, but the emission at 1.27 μm lives much longer. The right hand panel in Figure 2 shows that this long lived 1.27 μm component disappears when the sample is deoxygenated, proving that it is due to the singlet oxygen luminescence.

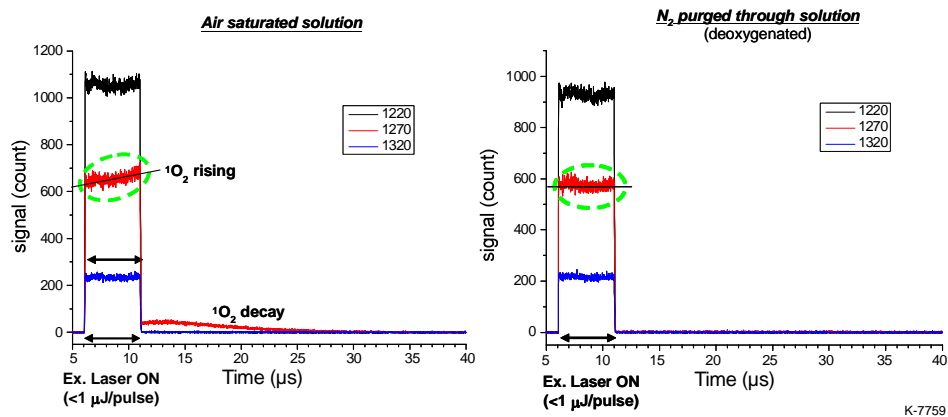


Figure 2. Temporal profiles of 10 μM BPD in PBS solution: air-saturated and deoxygenated solutions with each optical filter position. The deoxygenated sample demonstrates that the signal at 1.27 μm is due to singlet oxygen luminescence.

To help us develop and interpret our detection strategies, we developed a quantitative kinetic model⁸ for the long pulse diode laser excitation of the PS and the subsequent PS and singlet oxygen emissions as shown in Figure 3.

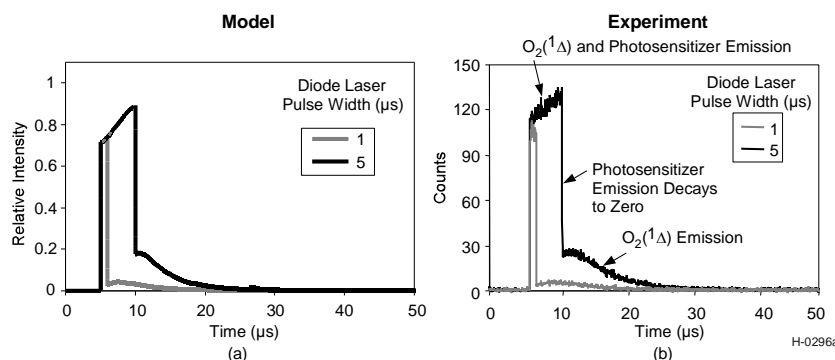


Figure 3. Temporal profiles for the radiative emission from singlet oxygen in water with different laser pulse widths: (a) prediction using our kinetic model with $\tau_T=1 \mu\text{s}$, $\tau_{\Delta\text{O}}=4 \mu\text{s}$, $\phi_T=0.4$, $\phi_{\Delta\text{O}}=0.7$; and (b) experimental results with chlorin e6 in aqueous solution. The τ_s and ϕ_s are the lifetimes and quantum efficiencies of the PS triplet state singlet oxygen (Δ) state.

Our previous work in developing a singlet oxygen imaging system¹⁰ used a state-of-the-art InGaAs camera with good sensitivity from 1.2 to 1.4 μm . However, that camera could only be gated at 30 Hz and was not capable of being used in a pulsed mode. Thus, we used it in a staring mode, but still used our pulsed diode laser PS excitation source. This limited us to using only spectral discrimination for extracting the singlet oxygen luminescence from the PS fluorescence. The camera was gated for three seconds at each of the three wavelengths (1.22, 1.27 and 1.32 μm) and integrated the optical emissions resulting from 30,000 laser pulses. Our model had indicated that the singlet oxygen luminescence in tissue would be between 3 and 5% of the PS fluorescence intensity at 1.27 μm *in-vivo* and this has been verified in our experimental studies.⁹⁻¹³

This approach was successful in obtaining initial images from mice with implanted tumors. However the signals were relatively weak and the signal to noise was marginal for imaging purposes. This was due in part to the continuum PS fluorescence described above. When the PS fluorescence is much stronger than the singlet oxygen luminescence, the linear interpolation between 1.22 and 1.32 μm to determine the singlet oxygen relative concentration breaks down as shown in Figure 4. The data in Figure 4 were obtained by replacing the three filters with a Cambridge Research Labs liquid crystal tunable filter (LCTF) with a bandpass of 20 nm at each wavelength. This is an excellent match to the linewidth of the singlet oxygen luminescence ($\Delta\lambda \sim 18 \text{ nm}$). Figure 5 shows that the simple linear fit of the NIR baseline (or background) works fairly well in a weakly quenching (methanol) *in vitro* environment. The green dotted line for the 2% IL solution is a polynomial fit through the out-of-the band signals. This method allows us to more accurately subtract the NIR background, and this produces a more accurate measurement of the singlet O_2 emission needed for *in vivo* measurements.

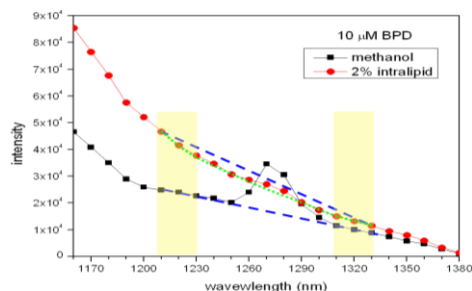


Figure 4. PS fluorescence background fits under the singlet O_2 emission spectral feature with 10 μM BPD in methanol and 2% intralipid solutions. The blue dotted lines are linear PS baseline interpolations between the 1.22 and 1.32 filters. The green dots show a polynomial fit to the out of band PS background.

Recently, we used an avalanche photodiode (APD) camera. We initially characterized the new APD camera to enhance the sensitivity of singlet oxygen detection sensitivity. It was developed for 3D LIDAR (Laser Identification and Ranging) and, as such, is capable of precise time gating. In LIDAR one uses the camera to measure the time of flight of a photon from a source to a target. Each of the pixels in the 32x32 array is a separate photon detector. Run in what is known as the Geiger mode, each avalanche InGaAs element has single photon detection capability (20% efficiency). The array can be gated at over 100 kHz and the gate width and delay can be set to precise values in software. This far exceeds any other

the counts in each image are plotted in Figure 7. Note that the images faithfully produced the time profiles similar to those shown in Figures 2 and 3 including the growth of the singlet oxygen during the laser pulse (1.27 μm filter).

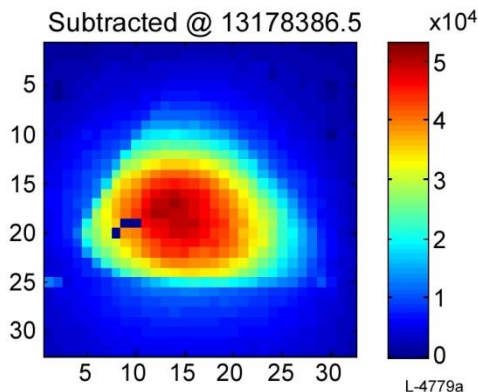


Figure 6. Singlet oxygen luminescence obtained with the APD camera. Excitation of the BPD 20 μM in methanol, was by 5 μs pulses at 40 kHz. The camera gate was set for 0.1 to 1 μs after the pulse. The number on top represents the sum of counts in all pixels for the image. Images were recorded at 1.22, 1.32, and 1.27 μm . The image shown is the result of the average of those recorded at 1.22 and 1.32 μm subtracted from that at 1.27 μm .

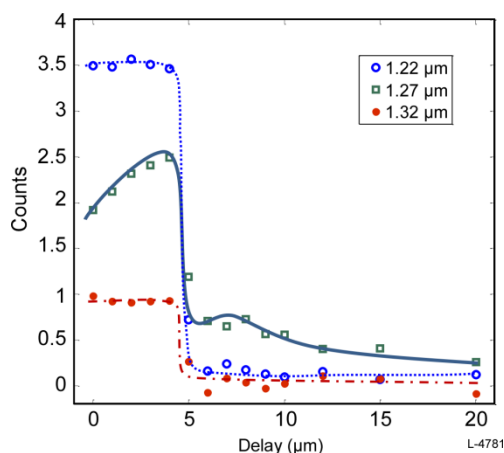


Figure 7. Composite of sums of counts within images recorded at three wavelengths and various gate positions.

2.3 *In-vivo* measurements

Cell Line and tissue Culture: A431, a human epidermoid carcinoma (ATCC, Manassas, VA, USA) were cultured in RPMI 1640 (Hyclone, Logan, UT, USA) 10% (v/v) Fetal Bovine Serum (Hyclone, Logan, UT, USA) and 100 IU/mL penicillin-streptomycin (Hyclone, Logan, UT, USA). Cells were grown in a humidified, 5% CO_2 , 37°C incubator.

Animals: All animal procedures were conducted according to a protocol approved by the Dartmouth Institutional Animal Care and Use Committee (IACUC). 6-8 week old female Athymic nude mice (NCI, Bethesda, MD, USA) were delivered to the Dartmouth Vivarium and housed for several days for acclimation. 1×10^6 A431 cells in a 1:1 mixture of media and matrigel (BD Biosciences, San Jose, CA, USA) were injected subcutaneously in a 50 μl volume into the flanks of the mice. Mice were placed on mouse purified diet (MP Biomedical, Solon, OH, USA) that allows for better fluorescent imaging by decreasing fluorescence in the mouse gained through the consumption of food. The tumors were allowed to grow up to 2 weeks when they reached optimal imaging size.

Imaging: Mice were kept in a surgical plane using isoflurane (3% for induction, 1-3% for procedure) using Dartmouth IACUC's approved procedures. The oxygen flow rate was at 1-2 L/min. A toe pinch was used to assess level of anesthesia, and mice were closely monitored for depth of anesthesia. The skin directly above the tumor was removed to reduce autofluorescence. To do so, a small incision was made 0.5 cm from the tumor. The skin was reflected and

removed from the tumor. This left the tumor on top of the muscles with blood perfusion, or attached to the skin itself. If the skin is free of tumor it was removed to expose muscle and tumor with a maximum 1 cm area around the tumor. If the tumor was attached to the skin, the skin with tumor was flipped over and sutured to another area of skin to expose the tumor, and muscle. Mice were first imaged for a control image, then injected with 1-3mg/kg Vertporfin Related Compound A (USP, Rockville, MD, USA) via tail vein, and imaged at specific time points. Mice were sacrificed as soon as imaging was complete, and mice never regained consciousness. Figure 8 is a photo of a mouse imaging experiment.

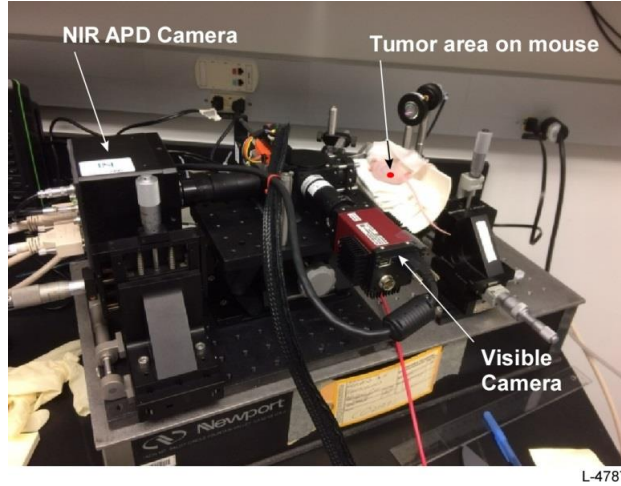


Figure 8. Imaging setup for *in-vivo* mouse with tumor on its flank.

In Figure 9 we show simultaneous images of BPD PS fluorescence and singlet oxygen luminescence recorded with the two cameras from one tumor on a mouse. The APD near-IR camera has an array of 32 x 32 pixels, each 100 x 100 μm . The visible camera (Pike F-145, 9.0 x 6.7 mm, 1392 x 1040 pixels, 6.5 x 6.5 μm pixel size) was used for the visible PS fluorescence measurement. Thus, the resolution is much higher for the visible PS images. These images map the singlet oxygen and PS distributions for a tumor about 3 mm across. The APD gate was 1 μs and began 500 ns before the end of the diode laser pulse. The images in Figure 9 were obtained 30 minutes after the injection of the BPD. Although the resolution of the near-IR image (< 200 μm) is inferior to the visible PS image, there is a clear correlation of the vascular structure and the pattern of PDT produced singlet oxygen as shown in the overlaid images.

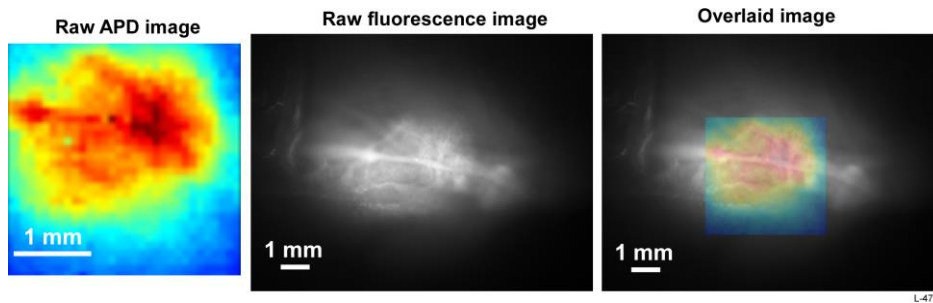


Figure 9. Comparison of singlet oxygen luminescence and PS fluorescence from a mouse tumor. Diode laser was run at 40 kHz with a 5 μs pulse width.

Figure 10 shows similar, simultaneous images of singlet oxygen and PS from a different mouse. However for this image, we replaced the pulsed diode laser with a conventional, cw, 690 nm diode laser; the intensity on the tumor was $\sim 100 \text{ mW/cm}^2$. The APD camera was gated at 100,000 fps with a 10 μs gate width. The refresh time for the camera is $\sim 2 \mu\text{s}$. To our knowledge, this is the first image of singlet oxygen in a macroscopic tumor, produced by a cw laser.

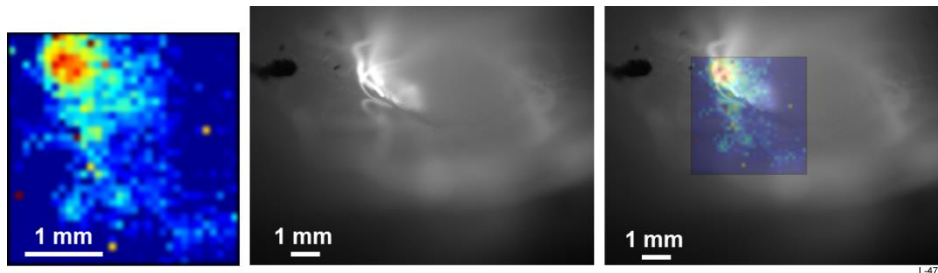


Figure 10. Images from a mouse obtained with a cw PDT diode laser.

2.4 Integrated imaging and point sensor

In more recent tests we have developed a more sensitive and comprehensive system: a Princeton Instruments NIRvana 640 camera, combined with an IR sensitive PMT, to provide both imaging and non-imaging capabilities. This new system also uses a cw laser source as used in conventional PDT treatments. This integrated dosimetry instrument has two simultaneous detection channels, i.e., an imaging channel that measures the spatial distribution of both the PS and singlet oxygen and a non-imaging channel that estimates the total amount of singlet $^1\text{O}_2$ generated during the PDT treatment. The two channels are complementary in that the imaging channel provides high spatial resolution while the non-imaging channel provides high spectral resolution and superior signal-to-noise ratio (SNR).

Figure 11 shows this integrated instrument. The entire system consists of portable rack mounted instrument that contains a laser source, desktop computer, and peripheral electronics, a box that contains the imaging setup, and a PMT signal detection unit. A fiber coupled 690 nm cw laser diode is used to excite the samples from the top side of the optical system at an oblique angle. The performance of the prototype dosimeter has been characterized quantitatively using tissue phantoms. It has also been successfully tested during animal studies in collaboration with Dartmouth College/Medical Center.

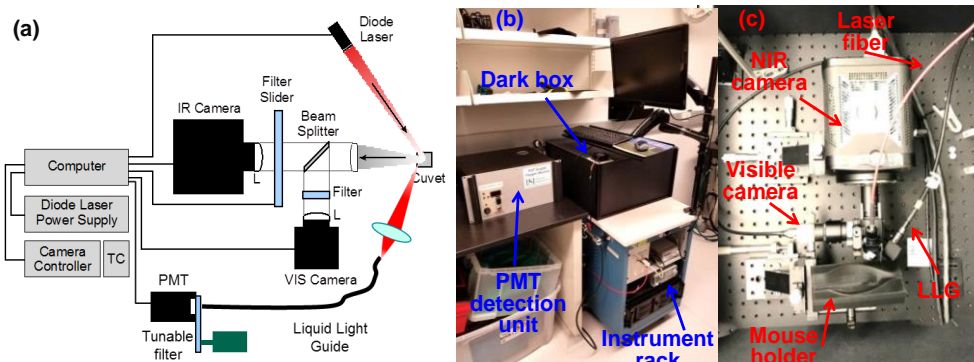


Figure 11. Optical singlet oxygen dosimeter. (a) Diagram of optical setup and control hardware. (b) Photo of instrument. (c) Photo of the optical setup.

The singlet oxygen imaging channel consists of a near infrared (NIR) camera (NIRvana640, Princeton Instruments), a CMOS visible-NIR camera (DCC3260M, Thorlabs), and a ~ 0.25 NA (numerical aperture), 1:1 magnification optical system. A dichroic mirror with a cutoff wavelength at 1050 nm is used to reflect ($>99\%$) the fluorescence signal below 1050 nm to the vis-NIR camera and to transmit ($>95\%$) of the signal above 1050 nm to the NIR camera. A bandpass filter (~ 15 nm bandwidth) centered at the 1270 nm is placed in front of the NIR camera to selectively transmit the singlet oxygen luminescence and block the out-of-band PS fluorescence. The signal collected by the NIR camera represents combined contributions from both singlet oxygen luminescence and PS fluorescence that is within the transmission band of the 1270 nm bandpass filter, i.e., $^1\text{O}_2 + \text{PS}$. A long pass filter cutoff at 700 nm is placed in front the vis-NIR camera that blocks the residual laser reflected from the sample back to the optical system. The fluorescence signal within the wavelength range of 700 nm – 1050 nm is detected by the vis-NIR camera, so that only PS fluorescence contributes to the vis-NIR image.

The nonimaging channel is composed of a liquid light guide (LLG), a liquid crystal tunable filter (LCTF), a NIR photomultiplier tube (PMT, H9170-45, Hamamatsu), and a single-photon counter. An aspheric condenser lens is used to collect the fluorescence signal from the tumor to the LLG, and a longpass filter cutoff at 1050 nm is placed in front of the LLG to block the scattered laser light and the PS fluorescence below 1050 nm. The transmission band of the LCTF is controlled by a graphic user interface system. By tuning the LCTF, the spectrum of the fluorescence signal in the wavelength range of 1180 nm – 1310 nm is measured. Figure 12(a) shows an example of how the $^1\text{O}_2$ signal intensity is quantified. Eight different wavelengths were measured, which each wavelength integrated for 6 s. The PS fluorescence background was calculated by fitting a cubic spline function to the first two and the last data points (red solid line in Figure 12(a), top). The $^1\text{O}_2$ fluorescence intensity was calculated by subtracting the fitted background from the data points and fitting a Gaussian lineshape to the subtracted values (Figure 12(a), bottom). The quantitative value for $^1\text{O}_2$ is the area under that Gaussian curve in counts. The sensitivity of the device was tested in different phantoms, which is shown in Figure 12(b). The device was sensitive enough to detect 1 μM BPD in PBS with a laser power of 39 mW. Under this condition, the total amount of the $^1\text{O}_2$ signal photons is $\sim 3\%$ of the total amount of PS fluorescence signal consistent with our earlier modeling⁸.

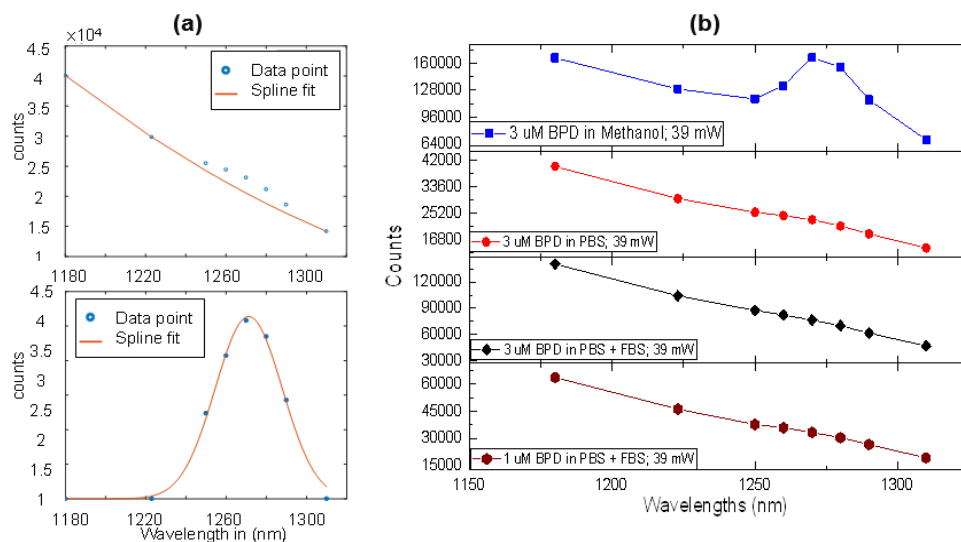


Figure 12. PMT based spectroscopic singlet $^1\text{O}_2$ measurement. (a) PS fluorescence (upper panel) and $^1\text{O}_2$ (lower panel) spectra of 3 μM BPD in PBS solution. Blue dots are PMT data points, and the red solid curve is a cubic spline fit to the first two and the last data point that simulates the PS fluorescence spectral shape (upper panel), and the Gaussian fit to the data points with PS subtracted is shown in the lower left panel. (b) Measured fluorescence spectra of different tissue phantoms showing PS and $^1\text{O}_2$ emissions.

We tested the performance of the imaging channel has during both phantom studies and animal experiments. Figure 13(b) shows the PS, PS+ $^1\text{O}_2$, and subtracted $^1\text{O}_2$ images of a tumor region of a living mouse. The singlet oxygen image shows the spatial distribution of the singlet $^1\text{O}_2$ generated during the PDT treatment. The mouse was injected with A431 squamous cell carcinoma (SCC) tumor cells two weeks prior to the experiment to develop solid tumors. During the experiment, the mouse was injected with BPD dye through tail vein. A 690 nm cw laser of ~ 39 mW was used to treat the tumor region.

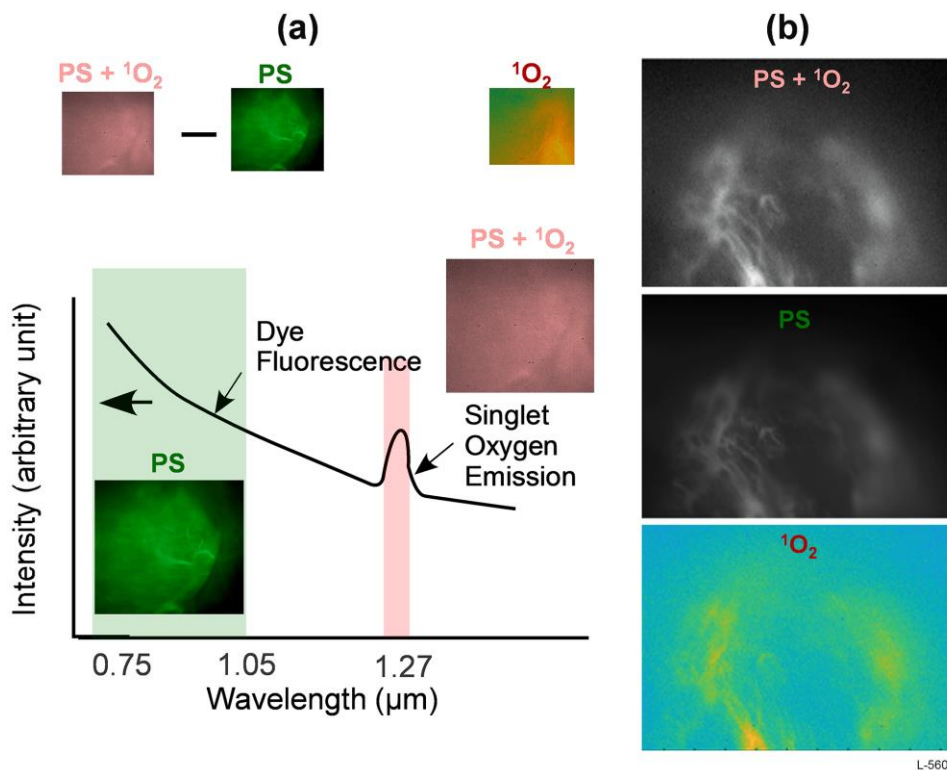


Figure 13. (a) Spectroscopic method for singlet $^1\text{O}_2$ imaging. (b) PS+ $^1\text{O}_2$ image captured by the NIR camera, PS image captured by the vis-NIR camera, and the subtracted $^1\text{O}_2$ image of a tumor laden mouse during cw PDT.

3. SUMMARY

The initial results of our integrated imaging and point sensor show promise for developing a sensitive dosimeter for both PS and singlet oxygen produced during PDT procedures. We have used cw diode lasers for this work to test whether our instrument is compatible with conventional PDT protocols that use cw light sources. We plan extensive animal studies with the goal of correlating tumor volume post PDT treatment with the singlet oxygen produced during the treatment. We also point out that our point, non-imaging sensor may also be a useful tool for PDT researchers and for early clinical applications.

4. ACKNOWLEDGEMENTS

This work was sponsored by the National Cancer Institute under grant numbers 1R43CA213607-01 and 5R44CA213607-03. The content is solely the responsibility of the authors and does not necessarily represent the official views of the National Institutes of Health. We are very grateful for this support.

5. REFERENCES

- [1] T. J. Dougherty, C. J. Gomer, B. W. Henderson, G. Jori, D. Kessel, M. Korbelik, J. Moan and Q. Peng, "Photodynamic Therapy," *J. of the National Cancer Institute* 90, 889 (1998).
- [2] M. Ochsner, "Photophysical and photobiological processes in the photodynamic therapy of tumors," *J. of Photochemistry and Photobiology B: Biology* 39, 1 (1997).
- [3] T. T. Goodell, S. L. Jacques and K. W. Gregory, "Evaluating Clinical Outcomes of PDT", *Proceedings of SPIE Vol: 4248*, 1 (2001).
- [4] "Optical Methods for Tumor Treatment and Detection: Mechanisms and Techniques in Photodynamic Therapy X," T. J. Dougherty, Editor, *Progress in Biomedical Optics and Imaging. Proceedings of SPIE, Vol. 4248*, San Jose, CA (2001). (Also see I-IX)

- [5] K. R. Wieshaupt, C. J. Gomer and T. J. Dougherty, "Identification of Singlet Oxygen as the Cytotoxic Agent in Photo-inactivation of a Murine Tumor", *Cancer Res.* 36, 2326 (1976).
- [6] D. Kessel, M. Castelli and J. Reiners, "On the Mechanism of PDT-induced Mitochondrial Photodamage," *Proceedings of SPIE Vol 4248*, 157 (2001).
- [7] V. H. Fingar, T. J. Wieman, S. A. Wichle and P.B. Cerrito, "The Role of Microvascular Damage in Photodynamic Therapy, The Effect of Treatment on Vessel Constriction, Permeability, and Leukocyte Adhesion", *Cancer Research* 52, 4914-4921 (1992).
- [8] Lee, S., L. Zhu, A. M. Minhaj, M. F. Hinds, D. H. Vu, D. I. Rosen, S. J. Davis and T. Hasan, T., "Pulsed Diode Laser-Based Monitor for Singlet Molecular Oxygen," *J. Biomed. Opt.* 13(3), 034010 (2008).
- [9] S. Lee, D. H. Vu, M. F. Hinds, A. Liang, T. Hasan and S. J. Davis, "Pulsed Diode Laser-Based Singlet Oxygen Monitor for Photodynamic Therapy: in-vivo Studies of Tumor-Laden Rats," *J. Biomed. Opt.* 13(6), 064035 (2008).
- [10] S. Lee, M. E. Isabelle, K. L. Galbally-Kinney, B. W. Pogue and S. J. Davis, "Dual-channel imaging system for singlet oxygen and photosensitizer for PDT," *Biomed. Opt. Express*, 2(5), 1233-1242 (2011).
- [11] S. Lee, S., K. Galbally-Kinney, B. A. Murphy, S. J. Davis, T. Hasan, B. Spring, Y. Tu, B. W. Pogue, M. E. Isabelle and J. A. O'Hara, "*In vivo* dosimetry: singlet oxygen emission and photosensitizer fluorescence," San Francisco, CA, SPIE Paper No. 7551-14, *Proc. SPIE*, Vol. 7551, 7510F (2010).
- [12] Srivalleesha Mallidi, Sriram Anbil, Seonkyung Lee, Dieter Manstein, Stefan Elrington, Garuna Kositratna, David Schoenfeld, Brian Pogue, Steven J. Davis, and Tayyaba Hasan, "Photosensitizer fluorescence and singlet oxygen luminescence as dosimetric predictors of topical 5-aminolevulinic acid photodynamic therapy induced clinical erythema," *J. Biomed. Opt.* 19(2), 028001 (Feb 06, 2014).
- [13] H. J. Laubach, S. K. Chang, S. Lee, I. Rizvi, D. Zurakowski, S. J. Davis, C. R. Taylor and T. Hasan, "In vivo singlet oxygen dosimetry of clinical 5-aminolevulinic acid photodynamic therapy," *J. Biomed. Opt.* 13, 050504 (2008).
- [14] M. M. Kim, R. Penjweini, T. C. Zhu (senior author): Evaluation of singlet oxygen explicit dosimetry (SOED) for predicting treatment outcomes of benzoporphyrin derivative monoacid ring A (BPD-MA)-mediated photodynamic therapy. *J. Biomed. Opt.* 22: 028002, Feb 2017 Notes: DOI:10.1117/1.JBO.22.2.028002.
- [15] M. T. Jarvi, M. S. Patterson and B. C. Wilson, "Insights into Photodynamic Therapy Dosimetry: Simultaneous Singlet Oxygen Luminescence and Photosensitizer Photobleaching Measurements", *Biophysical Journal* Volume 102 February 2012 661–671
- [16] T. J. Farrell, R. P. Hawkes, M. S. Patterson and B. C. Wilson, "Modeling of Photosensitizer Fluorescence Emission and Photobleaching for Photodynamic Therapy Dosimetry," *Appl. Opt.* 37(31), 7168-7183 (1998).
- [17] S. L. Jacques, "Simple Theory, Measurements, and Rules of Thumb for Dosimetry during Photodynamic Therapy", *Proc. SPIE*, Vol. 1065, 100-108 (1989).
- [18] B. W. Pogue, R. D. Braun, J. L. Lanzen, C. Erikson and M. W. Dewhirst, "Oxygen microelectrode measurements in R3230Ac Tumors during photodynamic therapy with verteporfin", *Proc. SPIE*, Vol. 4248, 144 (2001).
- [19] *Optical Methods for Tumor Treatment and Detection: Mechanisms and Techniques in Photodynamic Therapy XXIV*, D. H. Kessel and T. Hasan, editors, *Proc. SPIE*, Vol.9308 (2015).
- [20] *Optical Methods for Tumor Treatment and Detection: Mechanisms and Techniques in Photodynamic Therapy XXV*, D. H. Kessel and T. Hasan, editors, *Proc. SPIE*, Vol.99694 (2016).
- [21] B. W. Pogue, R. D. Braun, J. L. Lanzen, C. Erikson and M. W. Dewhirst, "Analysis of the heterogeneity of $^1\text{O}_2$ dynamics during photodynamic therapy with verteporfin," *Photochem. Photobiol.* 74(5), 700-706 (2001).
- [22] H. W. Wang, M. E. Putt, M. J. Emanuele, D. B. Shin, E. Glatstein, A. G. Yodh and T. M. Busch, "Treatment-induced changes in tumor oxygenation predict photodynamic therapy outcome," *Cancer Res.* 64(20), 7553-7561 (2004).
- [23] M. J. Niedre, A. J. Second, M. S. Patterson and B. C. Wilson, "In Vitro Tests of the Validity of Singlet Oxygen Luminescence Measurements as a Dose Metric in Photodynamic Therapy," *Cancer Research* 7986 (2003).
- [24] M. Niedre, M. S. Patterson and B. C. Wilson, "Direct Near-Infrared Luminescence Detection of Singlet Oxygen Generated by Photodynamic therapy in Cells In Vitro and Tissues in Vivo," 2002 American Society for Photobiology 0031-8655/02.
- [25] M. J. Niedre, C. S. Yu, M. S. Patterson and B. C. Wilson, "Singlet Oxygen Luminescence as an in-vivo photodynamic therapy dose metric: validation in normal mouse skin with topical amino-luvulinic acid," *British Journal of Cancer*, 92, 298 (2005).
- [26] B. W. Pogue, J. A. O'Hara, E. Demidenko, J. J. Wilmot, I. A. Goodwin, B. Chen, H. M. Swartz and T. Hasan, "Non-Vascular Targeting Photodynamic Therapy of the RIF-1 Tumor with Verteporfin Causes Enhanced Radiation Sensitivity" *Cancer Research*, 63, 1025-1033 (2003).

- [27] J. T. H. van den Akker, H. S. de Bruijn, G. W. J. B. van Henegouwen, W. M. Star, H. J. C. M. Sterenborg, "Protoporphyrin IX fluorescence kinetics and localization after topical application *Photochem. Photobiol.* 72(3) 399-406 (2000).
- [28] C. Sheng, P. J. Hoopes, T. Hasan, and B. W. Pogue (2007). "Photobleaching-based Dosimetry Predicts Deposited Dose in ALA-PpIX PDT of Rodent Esophagus." *Photochemistry & Photobiology* 83: 738-748.
- [29] I. W. Kim, et al., "direct measurement of singlet oxygen by using a photomultiplier tube-based detection system," *Journal of Photochemistry and Photobiology B: Biology*, 159: 14-23, June 2016.
- [30] M. M. Kim, et al., "PDT Dose Dosimeter for Pleural Photodynamic Therapy," March 2016, *Proc SPIE Int Soc Opt Eng.*, NIH PMC web site. <https://www.ncbi.nlm.nih.gov/pmc/articles/PMC4819254> (accessed August 21, 2017).
- [31] M. M. Kim, et al., "On the in vivo photochemical rate parameters for PDT reactive oxygen species modeling," *Physics in Medicine and Biology*, 62(5): R1-R48, March 7, 2017.
- [32] S. N. Letuta, et al., "Delayed luminescence of erythrosine in biological tissue and photodynamic therapy dosimetry" *Journal of Photochemistry and Photobiology B-Biology*, 163:232-236, October 2016.
- [33] I. Salas-Garcia, et al., "Photosensitizer absorption coefficient modeling and necrosis prediction during photodynamic therapy," *Journal of Photochemistry and Photobiology B-Biology*, 114: 79-86, September 3, 2012.
- [34] B. H. Li, et al., "Photosensitized singlet oxygen generation and detection: Recent advances and future perspectives in cancer photodynamic therapy," *Journal of Biophotonics*, 9(11-12): 1314-1325, Sp. Iss. SI December 2016
- [35] V. Sanchez, et al., "Physiological Considerations Acting on Triplet Oxygen for Explicit dosimetry in Photodynamic Therapy," *Photodiagnosis Photodyn Ther*, July 24, 2017.
- [36] B. Li, , et al., "Singlet oxygen detection during photosensitization," *Journal of Innovative Optical Health Sciences*, 6(1):1330002, 2013.